Flux spatial emission obtained from technical specifications for a general filament light source

Josep Arasa, Santiago Royo, Carles Pizarro, and Josep Martínez

A new, to our knowledge, method for evaluating three-dimensional flux distributions for general filament light sources is presented. The main advantages of the developed model are its generality and its simplicity. From plots of the emitted luminous intensity, usually provided by the lamp's manufacturer, in three orthogonal planes a detailed account is given of how to establish flux emission from the light source in any direction. The method involves a selective smoothing procedure, a curve-fitting step, and a final interpolation. A full model is developed for a typical commercial filament bulb (Philips, Model P21W Inco K) that is quite common in many industrial applications. A fourth intensity plot, usually provided by the lamp's manufacturer, is used to validate the model. To confirm the validity of the model further, we present an industrial application (the photometric simulation of a car taillight) that uses the modeled Philips Model P21W source. A comparison between simulated data obtained by use of the developed P21W model and measured results at our industrial partner's laboratories reinforces the proposed source model.

OCIS codes: 120.5240, 120.5630, 350.4500.

1. Introduction

Photometric models of light sources are crucial in optical design processes in which the amount of energy received in the final plane becomes critical. The way that luminous flux is distributed spatially usually imposes major restrictions on the whole system being designed. Although some techniques have been proposed for modeling optical systems with filament light sources, most of them refer to luminaire design. In such a field, the shape of the reflector involved is the main variable taken into account, so the design becomes focused more on the optical system than on the light source being used.[1,2]

Whenever photometric descriptions of stand-alone source emissions are considered they tend to rely on complex bases such as conglomerations of point emitters, axially normal subdivisions of the filament, or even more complex distributions.[3] This approach is troublesome as, for example, the shape of the filament plays a key role and this parameter has an appreciable and random variation from sample to sample. Furthermore, some of the hypotheses involved are difficult to justify from a physical point of view (e.g., the emission properties of each subdivision of the filament or how subdivisions interact with each other), so the luminous intensity in each direction is not easily obtained.

Our aim was to develop a solid model that is general enough to include the maximum number of light-source types by use of the simplest possible calculation procedure. If a model could be developed on the basis of the luminous-intensity plots in the three orthogonal planes that manufacturers usually provide (namely, the technical specifications of the lamp) the method would become general for any kind of source because such a method would be independent of the physical phenomena that cause the emission of light and would work on the basis of easily available data.

Such a model was developed in the present paper for the particular case of a filament lamp. This kind of source has certain drawbacks that are mostly inherent to the technical specifications being used but that might also appear in some other kinds of sources. First, these technical specifications usually show strong experimental dispersion as a result of the harsh manufacturing conditions for many of the elements involved. Furthermore, a simple analytical description of the curves that appear in technical

J. Arasa (arasa@oo.upc.es), S. Royo (royo@oo.upc.es), and C. Pizarro (pizarro@oo.upc.es) are with the Center for the Development of Sensors and Systems (CD6), Technical University of Catalunya, Violinista Vellsolà 37, E-08222 Terrassa, Spain. J. Martinez is with Yorka, Ltd., Venezuela 76, E-08019 Barcelona, Spain.

Received 4 February 1999; revised manuscript received 25 June 1999.

0003-6935/99/347009-09$15.00/0

specifications is not always obtained, which dictates the application of nonautomated curve-fitting procedures. Finally, a three-dimensional flux distribution has to be achieved from the curve-fitted intensity-emission distribution in the three orthogonal planes.

As an additional validation of the model, an industrial application that uses the source model dealt with in this paper is presented. The source model was applied to the design of taillights and indicators (hereafter referred to as pilots) for the automotive industry. The simulation of the photometric properties of the pilot as obtained from the geometrical computer-aided design (CAD) is compared with the experimental data obtained from the pilot's quality test at Yorka, Ltd. (Barcelona, Spain). The comparison of measured and simulated luminous-intensity values in a final plane reinforces the validity of our model.

In the following a methodology section introduces the steps that drive toward the desired lamp model, together with the available experimental data. Next, the results of applying the methodology to the initial data are presented step by step in Section 3 in which the final lamp model is obtained and validated. The results of using the proposed lamp model in an industrial application are then presented in Section 4.

2. Methodology

The model was developed in the steps outlined in Subsections 2.A–2.C.

A. Smoothing of the Initial Data

As stated in Section 1, our initial data were the manufacturer's technical specifications. The fact that these kinds of data are readily available for a number of light sources and suppliers gave our model the generality that we required.

To identify each of the planes present in the technical specifications, we needed to define an axis system to work with. Hereafter, the X axis is defined as the line connecting the bottom of the metallic connection of the lamp and the top of its glass cover; the Z axis defines the axis of symmetry of the filament (assuming the filament is a cylinder), and the Y axis is defined consistently (Fig. 1). Most manufacturers provide data in four independent planes, although only three of the planes (corresponding to planes defined as XY, XZ, and YZ) are needed to build the source model. The fourth plane is usually tilted 45° from the XY plane and contains the X axis.

Technical-specification data are usually measured far from the source (commonly 10 m away). This means that all intensity plots assume the sources to be a point located at the origin of the coordinates. However, the positions of the filament and the bulb must be kept in mind, as their orientations define the reference system. Furthermore, the position of the filament becomes relevant to the model because the intensity data present noticeable variations that depend on it. However, recall that, although the filament was used to define the reference system, alternative definitions may be used in other types of lamps without a loss of generality for the procedure, which is based in only the luminous-intensity plots.

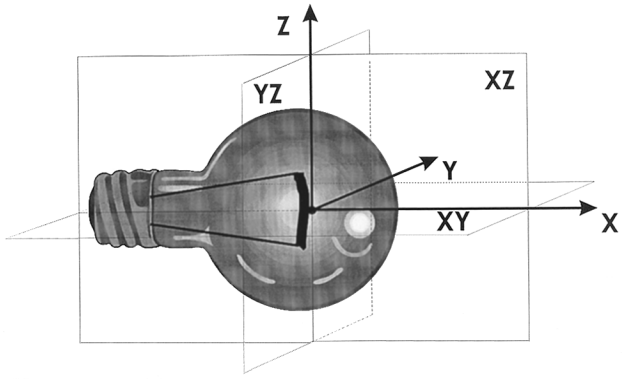

Fig. 1. Reference system described in the text. The X axis runs from the metallic base of the bulb to its glass top; the Z axis is determined by the axial direction of the filament; the Y axis is defined consistently. Although technical specifications refer to point sources, the lamp's position is used to define the reference system.

An example is developed on the basis of the Philips Model P21W Inco K (hereafter referred to as P21W) light source, a fairly common light source used in a number of industrial applications. However, the procedure for developing the model remains general. Figure 2 shows the technical specifications for the P21W light source that are needed to develop the model. The three plots correspond to planes XY, XZ, and YZ. The luminous-intensity data at each plane are described in reference to its polar coordinate with its origin on the right.

However, these technical specifications show major variations when different samples of the same model of lamp are considered (see Fig. 3). These variations may be caused by many uncontrolled effects that arise during manufacture, depending on the quality of the lamp, from small bubbles in the glass to different thicknesses or shapes of the filament. To make up for this effect, manufacturers either provide a smoothed general curve or, more often, provide plots for a number of independent samples.

If a smoothed curve is provided, the next step—the curve-fitting procedure—can be applied immediately. Otherwise, to achieve a representative average intensity plot, it is necessary for the number of samples provided to be great enough to remove the effects of the nonrepresentative values that may appear for individual samples.

Unfortunately, data are not usually provided for such a large number of samples. In our case only three different samples were available, as can be seen from Fig. 3. Therefore after data from the three available samples were averaged an additional smoothing procedure based on neighbor averaging was applied to remove the peaks and the valleys in each sample plot that were not representative of the mean intensity emission of the lamp. Figure 4 presents the data that correspond to a fourth plane,

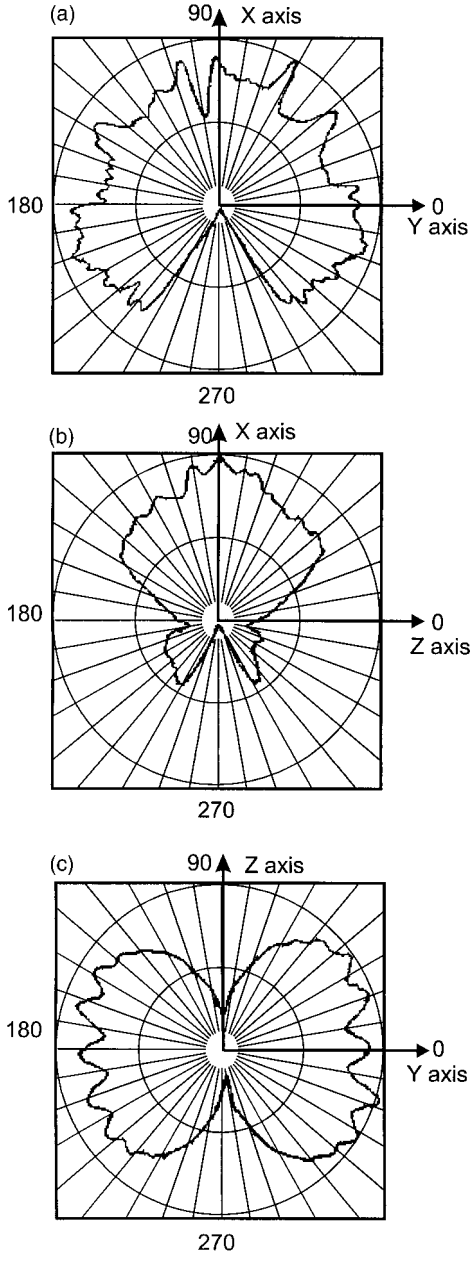

Fig. 2. Polar intensity plots provided by the manufacturer and used as data for building the model. The lamp is a Philips Model P21W Inco K: (a) plane *XY*, (b) plane *XZ*, (c) plane *YZ*.

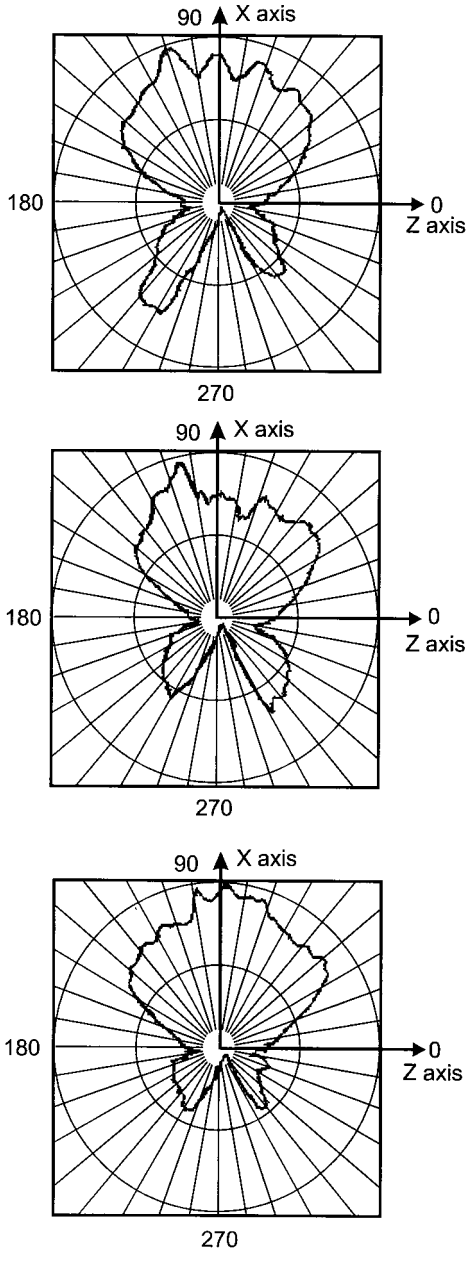

Fig. 3. Polar intensity plots for three different samples of the P21W lamp at plane *XZ*. Note that differences among the samples are significant, so smoothing through simple averaging would lead to incorrect results.

tilted 45° from the *XY* plane around the *X* axis, and that show the same kind of experimental dispersion that can be seen from Fig. 3.

B. Curve-Fitting Procedures

At this stage a smooth curve for each of the three orthogonal planes considered is already known. Our next step provides an analytical expression to describe the curve's shape across 360° for each of the planes in which data are known. Data points are plotted in a Cartesian representation rather than in the polar plot presented above.

Many curve-fitting procedures can be applied; in our case a commercial software program (TableCurve 2D) was used. A new problem arises from the complexity of the functions that appear: they frequently show more than one peak [see Fig. 2(b) or all the plots in Fig. 3, for instance], a characteristic that may be enough to pose problems for the automated features of the available curve-fitting software. This particular case deserves some attention because many lamps show distributions of this kind that might lead to complex fitting procedures.

As the three-dimensional reconstruction may lead to complex analytical solutions, a decision was made at this stage to impose fitting procedures in which a

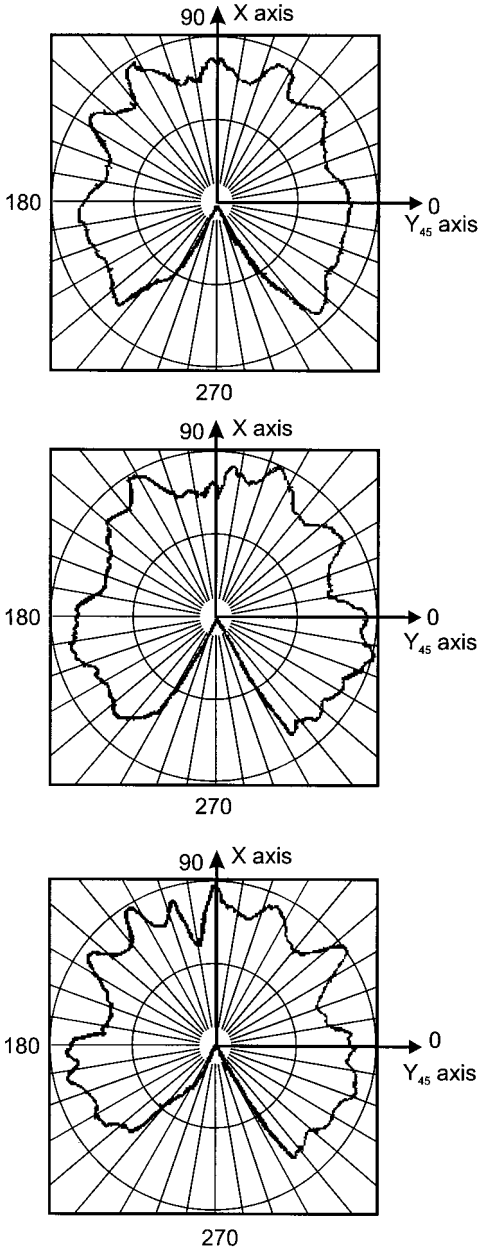

Fig. 4. Polar intensity plots for data on the fourth plane, tilted 45° from the Y axis. The plots are used as experimental data to validate the model. Axis Y_{45} is tilted 45° relative to the Y axis.

single analytical expression describes the intensity distribution in the plane considered. No analytical solutions that yield two different functions for the same plane (i.e., division of angular domains) were allowed, to avoid the unnecessary complexity they introduce into the calculations.

To fulfill this imposition, we applied a progressive curve-fitting procedure to these n-peaked curves. First, data were modified to curve-fit the first of the peaks; this was achieved by the arbitrary assignment of the values of the points not belonging to this first peak to the noise level. Then the original data were subtracted point by point from the data corresponding to the fitted equation for the first peak, which yielded a residual that contained the remaining peaks. An iterative data-modification, -fitting, and -subtraction procedure was then applied to each of the residuals until the final function was obtained as the sum of the analytical expressions from each curve-fitting step. The whole process is performed step by step in Subsection 3.B, where it is applied to the double-peaked curve in plane XZ that appears in the case of the P21W.

It must be noted that each plane is normalized at a different energy level in the specifications. A normalization was carried out to refer them to the same intensity value.

C. Interpolation Algorithm

At this stage an analytical function describing the source emission in planes XY, XZ, and YZ had been achieved. The next step was to develop an algorithm that would allow us to determine the luminous intensity in any direction in space.

Intensity emission in an arbitrary direction was calculated on a set of planes that shared the X axis and was tilted by $\alpha°$ relative to the XY plane. The curve on plane YZ was used as a weighting factor, giving a family of curves that continuously varied from the curve on plane XY ($\alpha = 0°$) to the curve on plane XZ ($\alpha = 90°$).

The value of the intensity from plane YZ that corresponds to a rotation of $\alpha°$ from the Y axis can be calculated from the analytical description of the source emission obtained through the procedures described in Subsection 2.B. This value is normalized from 0 to unity, referring to the maximum and the minimum, respectively, of the function describing the luminous intensity at the YZ plane $[f_{YZ}(\theta_{YZ})]$. Note that this means rotating the θ_{YZ} angle by $\alpha°$. This value weighted the ratio between the functions on XY $[f_{XY}(\theta_{XY})]$ and on XZ $[f_{XZ}(\theta_{XZ})]$. Let us say that

$$\xi = \frac{f_{YZ}(\alpha) - f_{YZ}^{(\mathrm{MIN})}}{f_{YZ}^{(\mathrm{MAX})} - f_{YZ}^{(\mathrm{MIN})}}, \tag{1}$$

$$f_{\alpha}(\theta_{\alpha}) = f_{XY}(\theta_{\alpha}^{XY})\xi + f_{XZ}(1 - \xi), \tag{2}$$

where $f_{\alpha}(\theta_{\alpha})$ is the light intensity in direction θ_{α} (which is the polar coordinate of a plane rotated by $\alpha°$ from the XY plane around the X axis) and θ_{α}^{XZ} refers to the direction of the projection of the tilted-plane coordinate (θ_{α}) on plane XZ. Obviously, the values obtained for tilts of 0° and 90° agree exactly with the functions on planes XY and XZ, respectively.

Here, however, a restriction is introduced to the model. This type of weighting process will be possible only in sources in which data on two planes coincide with the maximum and the minimum emission directions in the plane normal to both of them. This is usually the case for filament sources with the reference system described that, on plane YZ, show a minimum corresponding to the edge of the filament (coincident with plane XZ) and a maximum corresponding to its center (coincident with plane XY).

However, this requirement places a limitation on the application of this model to other types of light sources in which a different kind of intensity distribution on plane *YZ* would imply a different calculation of the weighting factor, as presented in Eq. (1) above. In other words, using Eq. (1) for the weighting factor implies that the intensity distribution on plane *YZ* has a maximum value that is coincident with plane *XY* and a minimum one that is coincident with plane *XZ*. This type of distribution is typical of filament lamps, as a decrease of the emitted intensity along the axial direction of the filament (defined as the *Z* axis) together with the maximum intensity emission along the defined *Y* axis are to be expected from this kind of source.

So our final model is a group of polar plots that are rotated (by any desired angle α) around the *X* axis, which is shared by all the polar plots. Each plot was calculated around the polar coordinate of each tilted plane. As a last step, the whole function volume was renormalized to be fitted to the total amount of energy emitted by the lamp.

D. Validation of the Model

Up to this stage, we used only data from the three orthogonal planes *XY*, *XZ*, and *YZ*. However, specifications usually provide data for some additional planes. Typically, as in the case of the Philips Model P21W that is developed here, additional data are provided for a plane tilted by 45° from the *Y* axis (see Fig. 4). Setting up a comparison between these experimental data and the values for that plane that are obtained from the model allows the validity of the light-source emission model to be tested.

3. Results

Results of the procedures described in Section 2 are presented now, starting from the provided experimental data.

A. Smoothing of the Initial Data

Figures 3 and 4 show that the experimental data from the supplier display strong deviations, depending on the sample used. As data were provided for only three samples, simple averaging of the data from the three samples and subsequent neighbor-averaging and smoothing techniques were applied to the data extracted from the technical specifications to remove the nonrepetitive peaks or valleys that appear in the data and are not common to all P21W lamps. Finally, the data were plotted on a Cartesian basis [relative intensity in normalized units (n.u.) against the polar angle in the corresponding plane] with the polar representation used by the lamps' manufacturer substituted in. The averaged and smoothed initial data for planes *XY*, *XZ*, and *YZ* are shown in this way in Fig. 5 in which the intensity values extracted from the technical specifications are plotted as circles in angular increments of 10°.

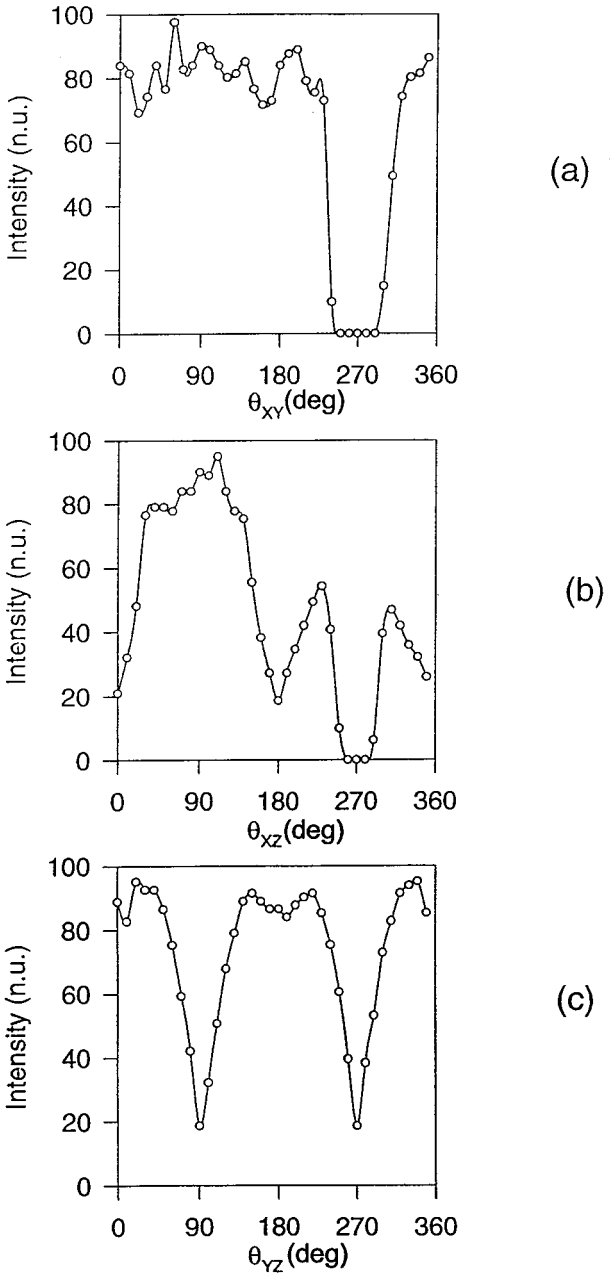

Fig. 5. Initial data from the curve-fitting process for the P21W example. Data from the technical specifications for three independent samples were averaged and smoothed for each plane and plotted on a Cartesian system instead of the original polar system. The circles represent data points. The intensity is plotted in normalized units (n.u.): (a) plane *XY*, (b) plane *XZ*, (c) plane *YZ*.

B. Curve-Fitting Procedures

A further simplification can be carried out if one takes advantage of the symmetry displayed by all the plots, as the curve-fitting need be performed for only half of the data in the plots. In Fig. 2 an axis of symmetry along the 90°–270° line can be appreciated in all plots. This may involve a 90° shift in the polar coordinate of the plane considered to set the axis of symmetry at 180° in the fitting procedures. Note how, in all planes, we keep only one function in the

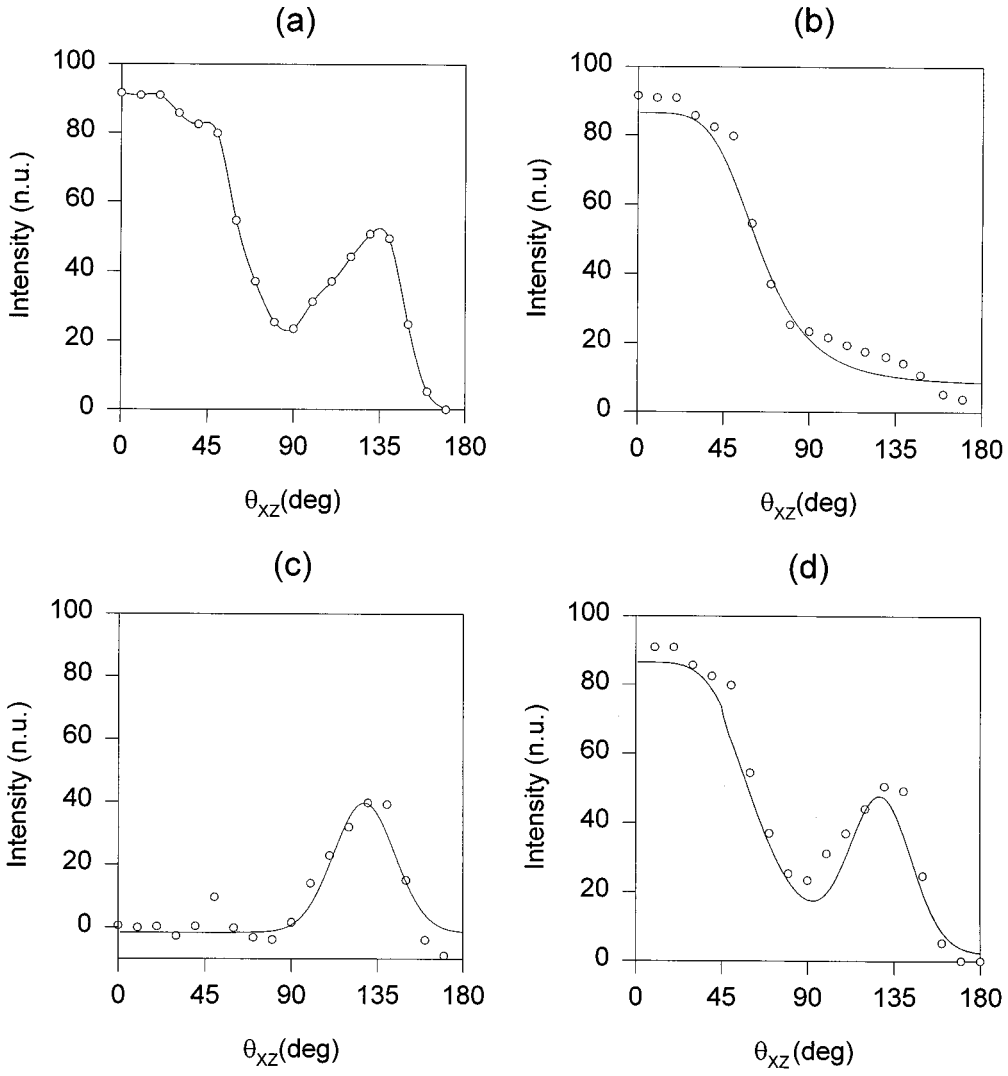

Fig. 6. Step-by-step fitting process for the data of plane *XZ*. In all cases a value of $\theta'_{XZ} = \theta_{XZ} - 90°$ was used to center the axis of symmetry of the curve. The intensity is given in normalized units (n.u.). (a) Initial data for the curve-fitting process [the data of Fig. 5(b) averaged on both sides of the axis of symmetry]. (b) Curve fitting of the data modified by the assignment of the data for the second peak to the noise level. (c) Curve fitting of the residual left by the subtraction of the initial data from the analytical expression for the first peak. (d) Comparison of the analytical sum of both curve-fitting steps with the initial data. Except for Fig. 6(a), the circles represent data points, and the solid curves represent the fitted functions.

whole plane, as desired. To compensate for minor local differences, we used data for fitting that were an average of the data on each side of the axis of symmetry. This process was adequate to obtain analytical solutions for the intensity on planes *XY* and *YZ* with automated commercial software.

However, no commercial software that was available to us was able to give a satisfactory analytical solution for data on plane *XZ* with automated curve-fitting procedures. The double peak on that plane prevented it from fitting adequately. An alternative fitting procedure that could cope with curves with more than just one peak was needed.

The whole process was described in Section 2 and is shown in Fig. 6. Except for Fig. 6(a), in all plots, the circles represent data points, and the solid curves represent the fitted functions. The data averaged for each side of the axis of symmetry of the curve [Fig. 6(a)] were modified by assignment of the second peak to the noise level and acquisition of an initial analytical expression, $f^{(1)}_{XZ}(\theta_{XZ})$ [see Fig. 6(b)]. The initial data were then subtracted from the corresponding analytical data, yielding a residual that consisted mainly of the second peak. Next, this residual was fitted, giving $f^{(2)}_{XZ}(\theta_{XZ})$ [Fig. 6(c)]. The sum of the two functions was then compared with the initial data to confirm the validity of the process performed [Fig. 6(d)].

As each specification is given in normalized coordinates relative to a different maximum in each plane, they must be normalized for them all to refer to the same intensity value. Figure 7 shows the polar plots that correspond to the analytical functions that describe the luminous intensity at planes *XY*,

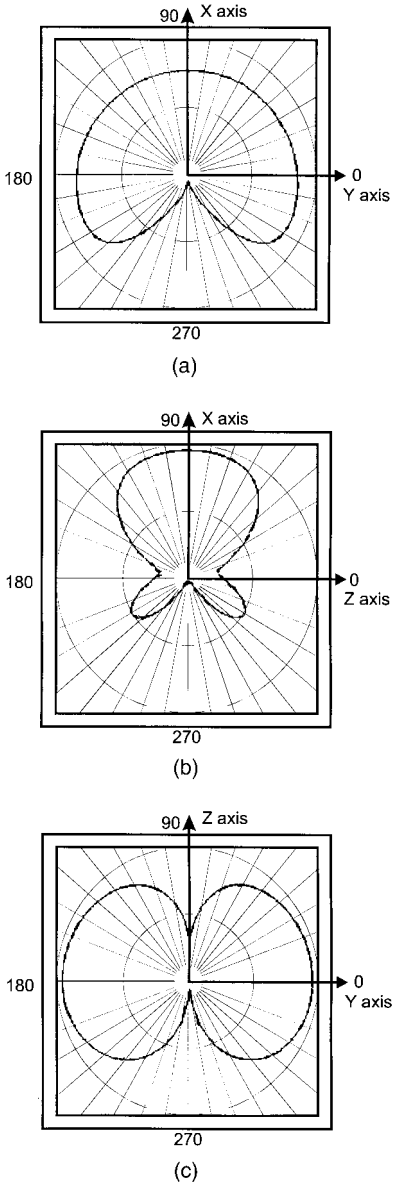

Fig. 7. Polar representation of the analytical values obtained from the curve fitting of (a) plane *XY*, (b) plane *XZ*, (c) plane *YZ*.

YZ, and *XZ*. Their analytical expressions are described below.

In plane *XY* [Fig. 7(a)], we have

$$I(\theta'_{XY}) = k_{XY}\left[a_{XY} + \frac{b_{XY}}{1 + \exp\left(-\dfrac{\theta'_{XY} - c_{XY}}{d_{XY}}\right)}\right], \quad (3)$$

where θ'_{XY} equals $\theta_{XY} - 90°$, a shift in coordinates whose purpose is to set the axis of symmetry at 0° for practical purposes. Note that, as desired, one analytical expression describes the function for all angular values, and consequently no computationally expensive subdivision of the domain has been carried out.

In plane *XZ* the use of two fitting steps yields a rather long expression [Fig. 7(b)]:

$$I(\theta'_{XZ}) = k_{XZ}\left\{a_{XZ} + \frac{b_{XZ}}{1 + (\theta'_{XZ}/c_{XZ})^{d_{xz}}} + e_{XZ} + f_{XZ}\exp\left[-\frac{1}{2}\left(\frac{\theta'_{XZ} - g_{XZ}}{h_{XZ}}\right)^2\right]\right\}, \quad (4)$$

where θ'_{XZ} is also shown as $\theta_{XZ} - 90°$.

Finally, in plane *YZ* the symmetry is so high that it allows a fitting in four quadrants [Fig. 7(c)], yielding

$$I(\theta_{YZ}) = k_{YZ}\left(\frac{a_{YZ} + b_{YZ}\theta_{YZ} + c_{YZ}\theta_{YZ}^2}{1 + b_{YZ}\theta_{YZ} + d_{YZ}\theta_{YZ}^2}\right). \quad (5)$$

Values for the constants involved in all expressions are listed in Table 1.

C. Interpolation Algorithm

The interpolation algorithm described in Subsection 2.C was then implemented to obtain the intensity distribution in any plane. When using the values derived for $I(\theta_{YZ})$ to obtain the weighting factor ξ the progression from the data in plane *XY* to the data in plane *XZ* took place smoothly and progressively [see Fig. 8(a)]. A simultaneous representation of a number of tilted planes can be seen in Fig. 8(b); a plane is plotted for each 30° of tilt. Tilting the plane in the desired direction allows the reconstruction of the intensity values in each spatial direction to be achieved. Axes are indicated in each graph. The hollow in the intensity emission caused by the edges of the filament and the hollow caused by the metallic support of the bulb can easily be identified in these plots. A final normalization must then be performed to adjust the total amount of energy calculated by the model to the total energy emitted by the lamp, yielding the multiplicative factor k_{ij} of Eqs. (3)–(5).

D. Validation of the Model

As explained, one of the specifications provided by the manufacturer was not used in the construction of the model. Therefore these experimental data for a plane tilted 45° from the *Y* axis provided us with an excellent tool for validating the model.

In Fig. 9 the data generated by the model (boldface

Table 1. Values for All Constants Used in Analytical Expressions (3)–(5) Fitted for Planes *XY, XZ,* and *YZ*[a]

Plane	*a*	*b*	*c*	*d*	*e*	*f*	*g*	*h*	k_{ij}
XY	2.110	79.985	139.07	−6.645					1.021
XZ	8.000	78.529	63.807	4.681	−1.668	41.300	128.03	16.016	1.051
YZ	42.210	-8.6×10^{-3}	0.689	1.2×10^{-3}	0.106				0.889

[a]Constants that are not used in analytical expressions (3)–(5) for the luminous-intensity data in planes *XY* and *YZ* are left blank.

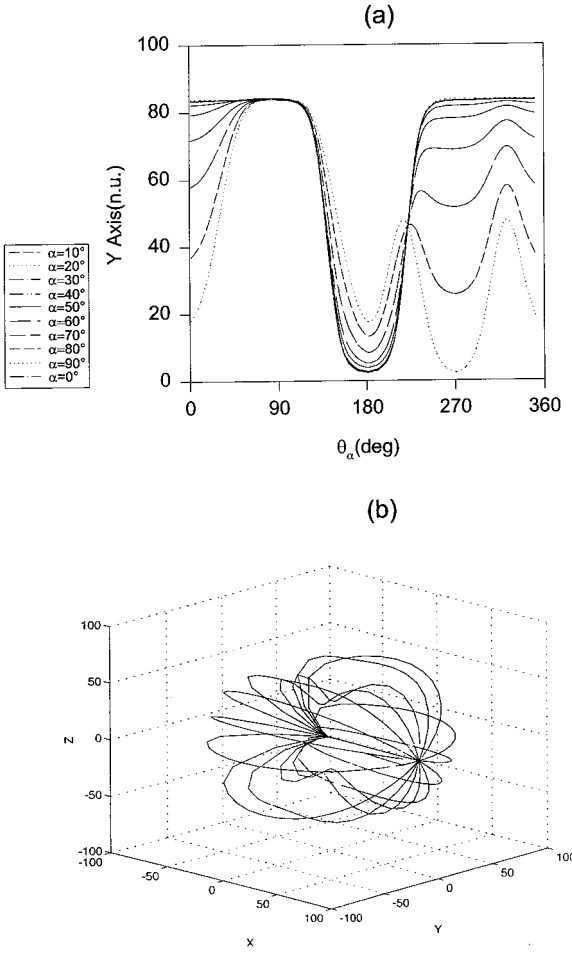

Fig. 8. (a) Cartesian representation of the transition of the intensity distributions from plane XY ($\alpha = 0°$) to plane XZ ($\alpha = 90°$). (b) Three-dimensional intensity distribution shown through tilted polar plots.

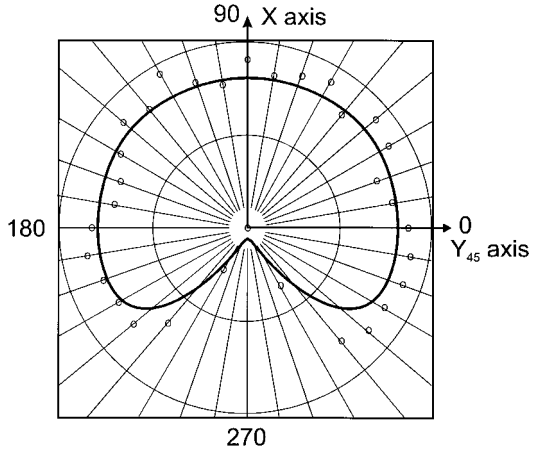

Fig. 9. Comparison of the analytically obtained and the provided values for a plane tilted by 45° from plane XY around the X axis. The two lightface complete circles represent 50% (inner circle) and 100% (outer circle) of the light intensity emission. The boldface closed curve represents the intensity values calculated by use of the proposed model, and the small open circles represent the experimental data points obtained from the technical specifications shown in Fig. 4.

curve) for the plane tilted by 45° and the smoothed data from the specifications shown in Fig. 4 (small open circles) for the same plane are compared. The experimental data in the tilted plane were smoothed in the same way as the data in each of the planes used in the construction of the model. It can be seen from Fig. 9 that the two sets of data agree with each other quite well, providing us with consistent proof of the validity of the model.

4. Application

The model presented here was applied to the simulation of car pilots at Yorka, Ltd. (Barcelona, Spain). By use of various sources (one of which was the P21W described here) and geometries a complete photometric simulation of Yorka, Ltd.'s new pilot design was

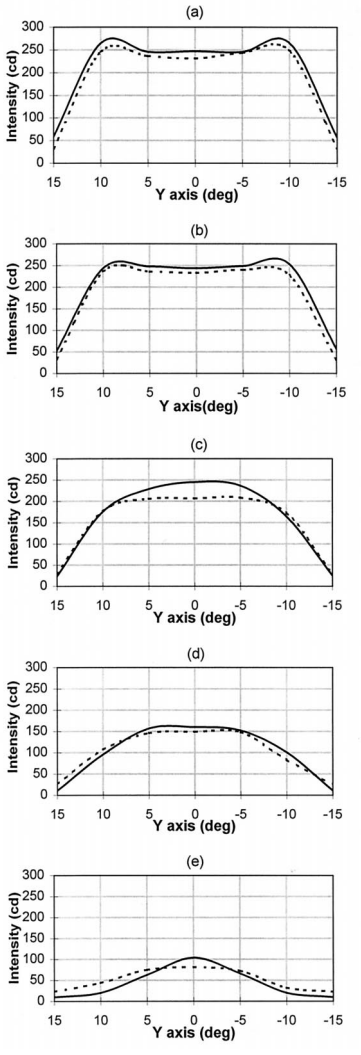

Fig. 10. Comparison between the simulated CAD photometric distribution (solid curve) and the experimental one (dashed curve) for a Peugeot T1 fog taillight. The source is the modeled P21W. The agreement of the two sets of data is an additional validation of the source model. Validation takes place at a plane located at $X = 10$ m. For practical purposes all distances are measured in degrees of elevation over the Y axis: (a) $z = 0°$ (corresponding to the Y axis), (b) $z = 2.5°$, (c) $z = 5°$, (d) $z = 7.5°$, (e) $z = 10°$.

carried out to avoid building expensive pilot prototypes to test the photometric validity of the designs.

A full application in a CAD outline was developed that, on the basis of the source model described and given the full complex geometry of the pilot, yields the energy distribution in the final measurement plane. The geometry involves the source position, a reflector, and a plastic colored molded lens with many lenslets described by NURBS (nonrational uniform B spline) geometry.

Data obtained from the CAD photometric simulation and experimental data from the Yorka, Ltd. workbench are compared in Fig. 10 for a Peugeot Model T1 fog light that consists of a paraboloidal reflector with a reflective metallic Leybold covering, the P21W modeled light source, and a lens made of Red Plexi 33690. The solid curves represent the simulated data, and the dashed curves represent the experimental data.

With our coordinate system kept based on the position of the lamp, the screen on which the measurements were made was a plane parallel to the *YZ* plane that was located at a distance from the light source of $X = 10$ m. Twenty pilot samples were measured to obtain a smooth experimental intensity plot. The five subplots shown are scans of the intensity values along lines parallel to the *Y* axis for different values of *Z*. *Z* is expressed in degrees of elevation over plane *XY* for production purposes. The data under plane *XY* are symmetrical. The measured and the CAD-simulated data agree very well in all planes for industrial requirements. The slight variations that can be seen in some planes are within the tolerances allowed in the manufacturing process of each single pilot.

5. Conclusions

A general model for obtaining spatial light distributions in filament sources has been developed. The model operates on the basis of the publically available technical specifications provided by manufacturers and performs three steps to build a model: an initial smoothing of the intensity data in three orthogonal planes, a curve-fitting procedure for the data in each plane, and an interpolation of the data from two of the planes relative to the third. A validation process for the model has been performed by use of the remaining data provided by the manufacturer (a fourth plane tilted by 45° from plane *XY* around the *X* axis). An additional validation was carried out through an industrial application that, on the basis of the proposed source model, performs fair photometric simulations for car taillights and indicators.

The limitation with filament sources lies in the weighting factor [Eq. (1)] of the interpolation algorithm because it relies on the particular form of the luminous-intensity data in plane *YZ*, which attain a minimum value on plane *XZ* and a maximum one on plane *XY*. Whenever data from the planes that correspond to the maximum and the minimum of the weighting function were not available from the manufacturer, the best solution has been to perform our own intensity measurements in those planes and then to define an appropriate weighting factor that takes into account the nonorthogonal directions of the maximum and the minimum intensity values in the plane used to calculate the weighting factor.

This project was carried out by the Department of Optics and Optometrics of the Technical University of Catalunya together with Yorka, Ltd., staff. Yorka, Ltd., also provided the required funding. The authors would also like to thank M. J. Yzuel for her interest and helpful suggestions.

References

1. R. Winston and H. Ries, "Nonimaging reflectors as functionals of the desired irradiance," J. Opt. Soc. Am. A **10,** 1902–1908 (1993).
2. J. C. Miñano and J. C. González, "New method of design for nonimaging concentrators," Appl. Opt. **31,** 3051–3060 (1992).
3. I. Powell and A. Brewsher, "Software development for design of illumination systems," Opt. Eng. **33,** 1678–1683 (1994).